



A review on the device efficiency limiting factors in Sb_2S_3 -based solar cells and potential solutions to optimize the efficiency

Mohaiyadeen Aliyar Farhana¹ · Arumukham Manjceevan² · Hong-Yi Tan³ · Chang-Feng Yan³ · Jayasundera Bandara¹

Received: 4 October 2022 / Accepted: 12 May 2023

© The Author(s), under exclusive licence to Springer Science+Business Media, LLC, part of Springer Nature 2023

Abstract

Thin-film photovoltaics based on earth-abundant and non-toxic Sb_2S_3 is the frontrunner material in thin-film solar cells due to its broad-band optical response and excellent electrical properties. Nevertheless, a PCE of ~28.64% has been projected for Sb_2S_3 solar cells, and the highest reported efficiency is ~8%. The poor performance of Sb_2S_3 -based solar cells is attributed to deep intrinsic traps that enhance recombination. Due to lattice dislocations, surface defects lead to sluggish charge transfer across interfaces and poor charge carrier mobility. A better understanding of the recombination losses in Sb_2S_3 bulk as an intrinsic layer and interfaces of Sb_2S_3 /electron transport and Sb_2S_3 /hole transport layers and transport mechanisms could lead to significant advancements in device performance. This review discusses the limitations of Sb_2S_3 -based solar cells based on theoretical and experimental studies, which will pave the way for future improvements in Sb_2S_3 -based solar cells.

Keywords Sb_2S_3 thin film · Thin-film solar cell · Limitations of Sb_2S_3 -based solar cells · Charge carrier recombination

1 Introduction

The increasing global energy demand leads to identifying and exploiting environmentally clean and renewable energy sources that can replace conventional energy resources (Suryawanshi et al. 2013; Chang et al. 2012). The solar energy that strikes the earth in one hour is enough to meet the world's annual energy consumption; hence, photovoltaic (PV) technology is at the forefront of converting solar energy into electrical energy at a

✉ Jayasundera Bandara
jayasundera.ba@nifs.ac.lk

¹ National Institute of Fundamental Studies, Hantana Road, Kandy 20000, CP, Sri Lanka

² Department of Chemistry, Faculty of Science, University of Jaffna, Jaffna, Sri Lanka

³ Guangzhou Institute of Energy Conversion, Chinese Academic of Sciences, No. 2 Nengyuan Road, Tianhe District, Guangzhou 510640, Wushan, China

rapid pace (Lewis et al. 2005; Dematage et al. 2014; Boix et al. 2011a; Chang et al. 2010; Manjeevan and Bandara 2016; Akilavasan et al. 2013; Todorov et al. 2013; Giordano et al. 2016; Zhou et al. 2018). The second-generation thin-film solar cells have continued to attract intensive research interest due to their high efficiency/cost ratio among single junction solar cells (Pastuszak and Węgierek 2022). Among them, in PCE, copper gallium indium sulfide (CIGS) and CdTe have achieved 23.4% and 22.0%, respectively (Gloeckler et al. 2013; Bosio et al. 2020; Hirai et al. 2013). Antimony sulfide (Sb_2S_3) is also one of the best candidates for thin-film solar cells since it possesses non-toxic elements compared to CdTe counterparts. Further, its constituent elements are highly abundant in nature. Sb_2S_3 exhibits an orthorhombic crystalline structure of the type Pnma. It shows a high absorption coefficient ($> 10^5 \text{ cm}^{-1}$) in the visible region. By generalized gradient approximation, Sb_2S_3 is a direct bandgap semiconductor in the crystalline stibnite form with an energy gap (E_g) of 1.76 eV (Ben Nasr et al. 2011). In direct bandgap semiconductors, the electron–hole pair can be produced relatively quickly due to the same electron momentum of valance and conduction bands. However, producing the electron–hole pairs in an indirect bandgap material with photon and phonon energy is possible. The production of electron–hole pairs in Sb_2S_3 could be faster than Si, whereas Si is an indirect bandgap semiconductor. Although, Si-based solar cells exhibit higher efficiency compared to others. The highest efficiency for Sb_2S_3 -sensitized solar cells is 7.5% for Sb_2S_3 planar (Choi et al. 2014a; Han et al. 2020). However, due to uninvestigated limitations in Sb_2S_3 solar cells, there is a large gap between the highest efficiency and theoretical efficiency of Sb_2S_3 planar solar cells (Kondrotas et al. 2018).

Although the Sb_2S_3 is a fascinating light-harvesting material, Sb_2S_3 -based solar cells' reported performance is inferior to other thin-film-based solar cells (Cai et al. 2020). The highest reported efficiency of ~8% (with an average V_{oc} , J_{sc} , and FF of in the range 400–600 mV, 12–18 mA/cm², and 50–60%, respectively) for Sb_2S_3 solar cells in planar configuration is much lower than the projected PCE efficiency of ~28% (with $J_{sc}=22.46 \text{ mA/cm}^2$, $V_{oc}=1.402 \text{ V}$, $FF=91\%$) under an AM 1.5G spectral irradiance for a single p–n junction with an absorber with 1.7 eV bandgap. Despite the enormous technological developments in the fabrication of defect-free photoactive layers with tunable physical properties, the efficiency of the Sb_2S_3 -based solar cell devices is far below the theoretical value (Kim et al. 2018; Zimmermann et al. 2015; Zhong et al. 2013; Zhang et al. 2018; Kriisa et al. 2015; Eensalu et al. 2019; Hong et al. 2018; Araújo et al. 2020; Wang et al. 2020). The drive towards enhancing efficiency beyond the value of 7.5% reported in 2014 by Choi et al. (Choi et al. 2014b) forms the basis of this review, which explores the significant and far-reaching theoretical and experimental efforts that have been expended to break this barrier or limit.

2 Limitation factors in Sb_2S_3 solar cell

The limitation factors of planar configuration based on the n-i-p device architecture comprising the ETM/ Sb_2S_3 /HTM configuration is mainly discussed in detail in this section. The device structure and the major charge carrier loss pathways for a n-i-p configuration of Sb_2S_3 based device are shown in Fig. 1a and b, respectively. These devices use a compact electron transport layer (ETL) coated on FTO and Ag or Au deposits on hole transport layer (HTL) as cathode and anode, respectively. The thin-film of Sb_2S_3 deposits on the ETM followed by HTL in n-i-p structure. Under illumination, the Sb_2S_3 on ETM absorbs sunlight

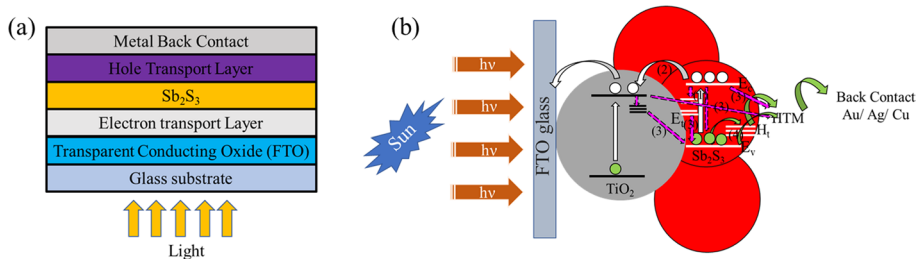


Fig. 1 **a** Schematic illustration of device architecture of thin-film Sb_2S_3 solar cell. **b** Schematic illustration of photoinduced charge-transfer processes (1) photo excitation of electron under illumination, (2) injection of electron towards Electron Transport Layer (ETL), (3) recombination pathways of excited electron, (4) Hole transport. Where E_c , E_v , E_t , H_t and H_{TM} referred the conduction band, the valence band, interface traps, hole traps and hole transport medium, respectively

and produce excited electron in the conduction band and hole in the valence band, followed by charge injections such as electrons and holes in the conduction band and valence band of Sb_2S_3 into ETM and HTL via tunneling process respectively.

Besides the extrinsic factors associated with the device structure and carrier transport limitations circumvented by the band alignment, factors intrinsic to the absorber layer have been found to affect device performance. These effects arise from optical losses or carrier trapping at the defect centers or levels (Zhao et al. 2021). Liping Guo et al. have identified numerous intrinsic defects in the Sb_2S_3 layer, such as Sb vacancy (V_{Sb}), S vacancy (V_{S}), S interstitial (S_{i}), and Sb and S antisites (Sb_{S} and S_{Sb}). These defects are the charge trap centers and recombination pathways (Guo et al. 2019). Therefore, the poor performance of Sb_2S_3 in these types of solar devices can be attributed primarily to intrinsically formed traps that enhance charge carrier recombination in bulk and at the surface/interface. However, it should be noted that the surface defect states can lead to longer carrier lifetime at interfaces and poor charge carrier mobility due to lattice dislocations and topological defects (Zeng et al. 2020; Mahuli et al. 2020; Chen and Tang 2020).

Efficiency enhancement can be accomplished through augmentation of the photon absorption. Several strategies have been explored, such as plasmonic-based nanostructures or quantum confinement methods that promote multiple exciton generation (Catchpole and Polman 2008; Ellingson et al. 2005). In this respect, quantum dots of Sb_2S_3 have been implemented in quantum dot-sensitized solar cells with 1.61% and 3.14% photoconversion efficiencies. More detailed discussions on this aspect can be found in Liang et al. (2018); Hsieh et al. 2015; Sun et al. 2020). However, compare to other thin-film solar cells and DSSC, only limited research has been conducted on the impact of transport mechanisms on device parameters of Sb_2S_3 -based solar cells, and the lack of such studies could be the reason(s) for not achieving significant progress on Sb_2S_3 solar cells (Farhana et al. 2023). A better understanding of the recombination losses in Sb_2S_3 bulk and interfaces of Sb_2S_3 /ETL and Sb_2S_3 /HTL, as well as transport mechanisms, could lead to significant advancements in device performance of n-i-p configuration assembled with Sb_2S_3 as an absorber. Hence, theoretical study and investigation of ultrafast self-trapping of photo-excited carriers may facilitate the development of Sb_2S_3 thin-film-based solar cells. Several research groups (Cai et al. 2020; Courel et al. 2019; Cao et al. 2020; Xiao et al. 2020; Islam and Thakur 2020) have recently reported on the theoretical or simulation of minority carrier lifetime, interface recombination, and different transport mechanisms of Sb_2S_3 thin-films,

while several other research groups (Christians et al. 2013, 2014; Lee et al. 2013; Yang et al. 2019; Grad et al. 2021; Lian et al. 2021; Li et al. 2021) have reported on the experimental investigation of excited-state carrier dynamics and defect properties in Sb_2S_3 . In this review, we discuss the limitations of Sb_2S_3 -based solar cells based on theoretical and experimental studies, which will pave the way for future improvements in Sb_2S_3 -based photovoltaic solar cell performance.

2.1 Experimental study

The experimental investigation of the critical factors such as the carrier conductivity, lifetime, diffusion coefficient, diffusion length of the exciton, chemical capacitance, recombination resistance, and defects, affects the photoelectric behavior of Sb_2S_3 solar cell is indispensable for the improvement of their performance (Boix et al. 2011a, 2011b). In a recent review, the device performance and the optimization of the structure and morphology of the light-harvesting Sb_2S_3 layer has been discussed (Farhana et al. 2023). Doping of Sb_2S_3 , surface passivation, band alignment optimization, and defect passivation are the most studied techniques to improve the device's performance (Han et al. 2020; Xiao et al. 2020; Myagmarsereejid et al. 2021; Aliyar Farhana and Bandara 2022; Shang et al. 2016). However, the conversion efficiency of the Sb_2S_3 solar cell remains at 7.5% as the optimization has been mostly limited to the Sb_2S_3 structure and a smaller number of research performed on critical factors such as carrier transport and recombination. Depth analysis of carrier transport and recombination were first reported by (Christians et al. 2013) and (Boix et al. 2011a, 2011b). In an early study by Christian et al., the fate of photogenerated holes and diffusion of holes were investigated by femtosecond transient absorption spectroscopy. It was identified that holes captured by sulfur form a sulfide radical ($\text{S}^{\bullet-}$) in the crystal lattice, and then holes transferred from the Sb_2S_3 absorber to the CuSCN hole conductor with an exponential time constant of 1.68 ns as shown in Fig. 2a. The recombination in Sb_2S_3 is reported to be the main limiting factor in determining PCE performance in Sb_2S_3 -based solar cells, emphasizing the importance of having a well-crystalline and defect-free Sb_2S_3 coating or surface treatments to mitigate recombination losses. According to Christian et al. et al., hole transfer across the Sb_2S_3 -CuSCN interface is critical and must be highly efficient in order to improve solar cell performance because hole accumulation in the absorber species due to slow hole-transfer at the Sb_2S_3 -HTL interface increases the recombination at the TiO_2 - Sb_2S_3 interface. (Christians et al. 2013) To mitigate the buildup of holes in Sb_2S_3 , surface modification at the Sb_2S_3 /CuSNS interface is vital for the optimization of efficiency.

According to Boix et al., hole transfer across the Sb_2S_3 -HTL interface and hole diffusion in the Sb_2S_3 absorber layer play a significant role in device performance (Boix et al. 2011b). It was clearly demonstrated in their study that minority carrier diffusion length and interfacial hole-transfer are important parameters that limit the device performance for a thicker Sb_2S_3 layer (20–130 nm), whereas interfacial hole-transfer, rather than mobility, is the most important parameter limiting the device performance of a thin Sb_2S_3 layer (Christians et al. 2013, 2014). Hence, for further optimization of these photovoltaic, the importance of having a critical Sb_2S_3 thickness beyond the optimum value in which charges are no longer extracted efficiently has been demonstrated in this study (Boix et al. 2011a). By Impedance spectroscopy (IS) analysis, Boix et al. also demonstrated that lower charge recombination in planar polycrystalline Sb_2S_3 thin-film solar cells could be expected due to lower effective surface area and consequently higher V_{oc} and J_{sc} (Grad et al. 2021).

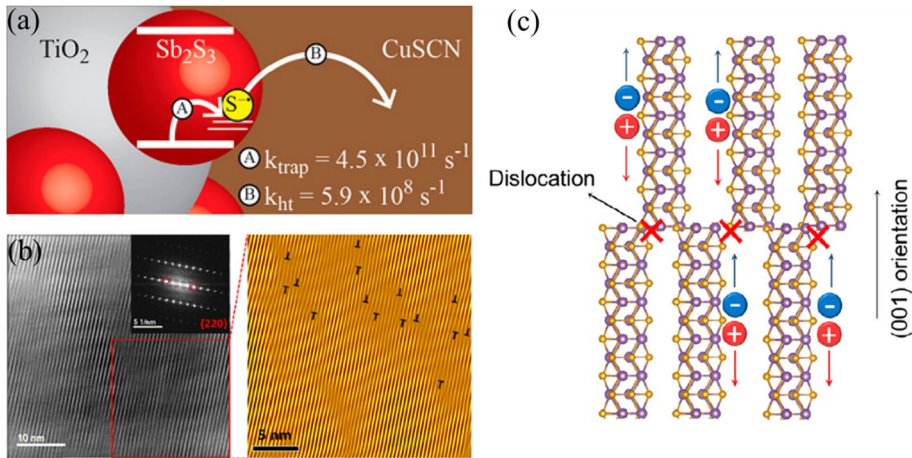


Fig. 2 **a** Energy level diagram of TiO₂/Sb₂S₃/CuSCN ETA solar cell showing transfer of photogenerated holes from the absorber species to the p-type hole conductor, Reproduced with permission, Christians et al. (2013) **b** Filtered high-resolution TEM images (left), electron diffraction patterns (inset of left), and color-coded inverse FFT images from the selected pair of reflection spot red-circled in the FFT images of Sb₂S₃. The label “T” was used to mark the dislocation core, which points the direction of the additional columns. Reproduced with permission, Li et al. (2021), **c** Schematic diagram of the carrier transport near the dislocations along (001) orientation of Sb₂(S,Se)₃ materials. Reproduced with permission, Li et al. (2021)

However, it is predicted that the increase in hole transport resistance in the HTM is due to the reduction in the screening of charges in holes in planar Sb₂S₃ devices affecting the total series resistance of the cell and reducing the FF (Boix et al. 2011b).

Although carrier mobility is one of the most fundamental electronic parameters influencing overall performance, studies of carrier transport in Sb₂S₃-based devices are scarce, and to optimize the device performance of Sb₂S₃-based solar cells, the investigation of majority carrier mobility is imperative. The majority carrier transport in a working Sb₂S₃ device has been reported by Li. et al. using the defect-resolved mobility measurement (DRMM) method, in which they reported that even with the preferred [hk1] crystalline orientation, which could be beneficial for better carrier transport, Sb₂S₃ suffers from low carrier mobility, resulting in high bulk resistance and poor carrier collection efficiency (Li et al. 2021). As the measured conductance of Sb₂S₃ is low, the corresponding effective majority carrier mobility has been reported to be surprisingly as low as $10^{-5} \text{ cm}^2 \text{ V}^{-1} \text{ s}^{-1}$, which has been partly attributed to the high anisotropy ribbon-like structure, that restricts inter-ribbon carrier transport between the (Sb₄Se₆)_n or (Sb₄S₆)_n ribbons due to distortion of the periodic lattice of a one-dimensional crystal which is known as Peierls distortion (Kondrotas et al. 2018; Zhou et al. 2015; Zeng et al. 2016). On the other hand, dislocations which are also predicted to be deep electronic trap states constraining the minority carrier lifetime in Sb₂S₃ grains, have been reported to obstruct the carrier transport path as each dislocation may act as a dead-end for both electron and hole transport (Fig. 2b, c).

To mitigate the formation of dislocations, stress control growth by using advanced growth processes has been suggested (Kondrotas et al. 2018). Since Sb₂S₃ is an orthorhombic crystal structure, there are three independent components of linear dielectric tensor. The dielectric constant (ϵ) is decreasing with increasing frequency because of decreasing orientation polarization. Due to the interfacial polarization, ϵ reach a constant value at high frequency. The dielectric constant at high frequency was found at 9.29434, 131.547, and

126.892 in x, y, z directions, respectively (Radzwan et al. 2017). Another study reported that the dielectric constant of Sb_2S_3 is 7.08 (Kumar and Kumar 2020). The reported short carrier diffusion length in Sb_2S_3 has been attributed to the higher recombination of excited electrons in Sb_2S_3 n-i-p planar or sensitized structure. The fully depleted absorber has been suggested to mitigate the constraints of fill factor and carrier collection efficiency of Sb_2S_3 solar cells caused by low carrier mobility. As the built-in electric field in the n-i-p device structure is applied to the entire absorber layer, carrier transport efficiency and as a result, power conversion efficiency can be enhanced. Hence, in order to significantly improve the effective carrier mobility of Sb_2S_3 and Sb_2Se_3 , it is critical to not only modify the grain orientation further, but also to reduce crystalline defects within the grains because the dislocations are commonly distributed in the grains.

Li et al. reported that defects (extrinsic or intrinsic) in Sb_2S_3 film detrimentally affects the solar cell performance. By optical deep-level transient spectroscopy investigation, Lian et al., reported three electron traps, E1, E2, and E3 (donor defects), with energy levels of 0.31, 0.60, and 0.69 eV below the conduction band minimum (CBM) in Sb-rich Sb_2S_3 film. (Lian et al. 2021). While in the S-rich Sb_2S_3 film (Fig. 3a(i)-(ii)), two-hole traps H1 and H2 (acceptor defects) with energy levels of 0.64 and 0.71 eV above the valence band maximum (VBM) were reported. These traps E1, E2, E3, H1, and H2 have been attributed to Sb-interstitial (Sb_i), S-vacancy (V_S), Sb_S antisite, Sb-vacancy (V_{Sb}), and S_{Sb} antisite defects, respectively (Cai et al. 2020; Guo et al. 2019). It has been reported that defects V_S and Sb_S predominant in Sb-rich Sb_2S_3 whereas V_{Sb} (major) and S_{Sb} antisite (minor) appear in S-rich conditions, and these defects act as carrier traps/ recombination sites as the energy level of these deep-level defects are more than 0.3 eV far from CBM or VBM (Lian et al. 2021). Traps E2 and E3 in Sb-rich Sb_2S_3 (Table 1), were reported to enhance the charge recombination due to large capture cross-section and high trap density, whereas traps H1 and H2 in S-rich Sb_2S_3 were found to suppress charge recombination and prolonged the charge carrier lifetime due to small capture cross-section and low trap density. Hence, in Sb-rich Sb_2S_3 film, inefficient extraction of trapped photo-excited carriers leads to pinning the electron quasi-Fermi level near traps E2 and E3, whereas in S-rich conditions, the pinning effects are reduced, resulting in improved V_{OC} pinning effects (Lian et al. 2021). Therefore, the next breakthrough efficiencies of Sb_2S_3 could be with S-rich Sb_2S_3 film that suppresses V_{Sb} without introducing new deep-level defects. Similarly, Lee et al. reported an interface trap around $E_c - 1.03$ eV below the conduction band edge of Sb_2S_3 based on deep-level transient spectroscopy (DLTS) analysis and its role as are recombination center for carriers generated from Sb_2S_3 QDs (Fig. 3b). (Lee et al. 2013).

In recent years, Yang et al. and Grad et al., investigated the time-resolved transient absorption (TA) and time-resolved two-photon photoemission (tr-2PPE) measurements to access the major energy loss mechanisms in planar Sb_2S_3 solar cells. It was reported that the experimentally observed excited state carrier lifetimes are barely explainable by an extrinsic defect trapping mechanism caused by extrinsic defects such as surface/interface/bulk defects. (Yang et al. 2019; Grad et al. 2021) By performing absorption and photoluminescence spectroscopy studies together with time-resolved TA measurements of polycrystalline Sb_2S_3 film and high-quality stoichiometric Sb_2S_3 single crystals, Yang et al., strongly suggested that the losses can be attributed to low charge carrier mobility due to intrinsically self-trapping of photo-excited carriers in Sb_2S_3 by lattice deformation (Yang et al. 2019). As self-trapping is common in materials with small elastic constant, self-trapping is possible with Sb_2S_3 as the calculated elastic constant of Sb_2S_3 is small (~ 40) (Landau 1933; Koc et al. 2012). As Sb_2S_3 has a soft lattice with quasi-1D crystal structure composed with $(\text{S}_4\text{S}_6)_n$ ribbons stacked with van der Waals interaction, free carriers

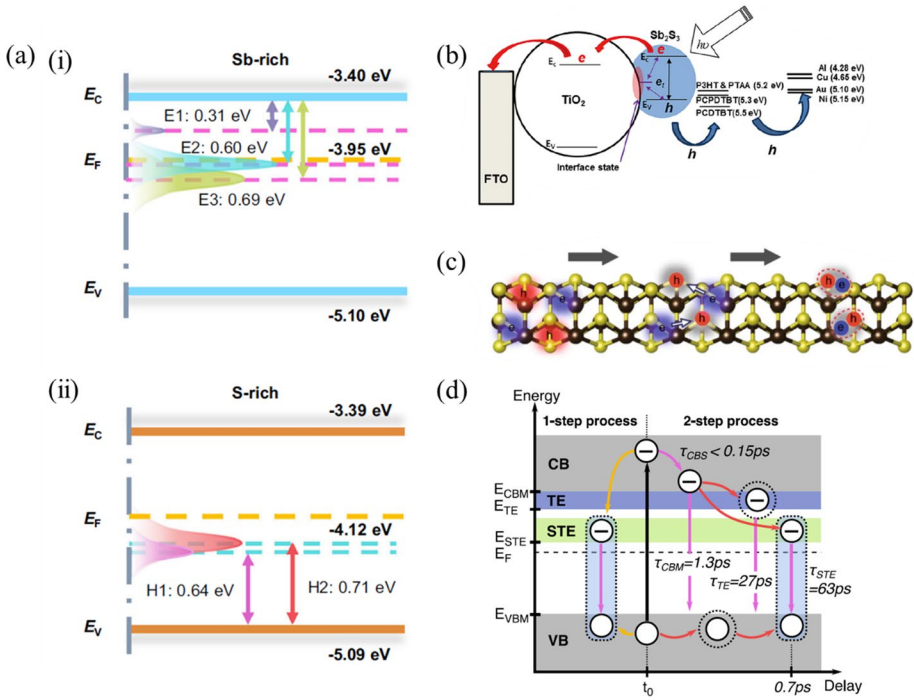


Fig. 3 a Schematic of band structure. (i), (ii) Conduction band (E_C), valence band (E_V), Fermi level (E_F), and trap energy level (E_T) for Sb-rich and S-rich Sb_2S_3 films. Reproduced under terms of the CC-BY license, Lian et al. (2021) b An illustration of carrier transport from the Sb_2S_3 QDs to the FTO electrode and carrier capture process into the defect state in the inorganic–organic heterojunction Sb_2S_3 QD solar cell. Reproduced with permission, Lee et al. (2013) c Self-trapping process. a Scheme showing two-step formation process of STEs in Sb_2S_3 : hole is self-trapped first and then electron is captured by trapped hole to form STE. Reproduced under terms of the CC-BY license, Yang et al. (2019) d Relaxation pathways and self-trapping: At t_0 an electron is excited from the VB to the CB due to absorption of a pump photon. In the 1-step process the photogenerated electron–hole pair is immediately trapped by local lattice distortions and forms a self-trapped exciton (STE). In the 2-step process, a free electron and hole are trapped separately within the lattice before they merge to form a STE. The trapping of free charge carriers is marked by red and orange arrows, and charge carrier relaxation is indicated by pink arrows. The measured time constants are indicated. Reproduced under terms of the CC-BY license, Grad et al. (2021).

Table 1 Deep-level defect parameters (trap type, trap energy level (E_T), capture cross section (σ), trap density (N_T), carrier lifetime (τ), shallow donor concentration (N_S)) of Sb-rich and S-rich Sb_2S_3 films. Reproduced with permission Lian et al. (2021)

| Sample | Trap | E_T (eV) | σ (cm^2) | N_T (cm^{-3}) | τ (ns) | N_S (cm^{-3}) |
|---------|-------|-----------------------|---------------------------------|--------------------------------|--------------------|----------------------------|
| Sb-rich | E_1 | $E_C - 0.31 \pm 0.02$ | $(0.54 - 8.13) \times 10^{-17}$ | $(3.75 - 5.63) \times 10^{14}$ | 2.18×10^3 | 7.71×10^{16} |
| | E_2 | $E_C - 0.60 \pm 0.02$ | $(0.26 - 4.68) \times 10^{-16}$ | $(1.57 - 3.31) \times 10^{15}$ | 6.46×10^1 | |
| | E_3 | $E_C - 0.69 \pm 0.02$ | $(0.11 - 1.75) \times 10^{-15}$ | $(1.38 - 2.01) \times 10^{15}$ | 2.84×10^1 | |
| S-rich | H_1 | $E_C + 0.64 \pm 0.01$ | $(0.46 - 1.31) \times 10^{-15}$ | $(0.45 - 1.58) \times 10^{15}$ | 4.83×10^1 | 5.13×10^{16} |
| | H_2 | $E_C + 0.71 \pm 0.02$ | $(0.49 - 1.17) \times 10^{-16}$ | $(6.71 - 8.57) \times 10^{14}$ | 9.97×10^2 | |

can be trapped within potential wells produced by local lattice distortion. Later, Grad et al. confirmed the intrinsically self-trapping states in 1-D Sb_2S_3 by using time-resolved two-photon photoemission (tr-2PPE) experiments carried out to identify the loss mechanism in the (100) surface of a cleaved Sb_2S_3 single-crystal (Grad et al. 2021). Based on ultrafast relaxation measurements, as shown in Fig. 3c and d, the authors proposed a self-trapping model in which, after photoexcitation of an electron-hole pair, the conduction band minimum (CBM) has been observed in less than 150 fs and self-trapping of free carriers by the depopulation of the CBM within 1.3 ps. Consequently, these electrons in the CBM get trapped by phonons (to form polarons), causing the electrons to slightly lower their energy and form self-trapping of electrons (TE) or captured by trapped holes to form self-trapped excitons (STE). The TE and STE states were reported to be located in the band gap at 0.06 eV and 0.44 eV below the conduction band minimum, respectively, with charge carriers having long lifetimes of 27 ps and 63 ps, respectively. Hence the losses can be attributed to low charge carrier mobility as a result of self-trapped charge carriers in gap states have longer lifetimes. It was found that the trap states are intrinsically formed in 1D material. As the major energy loss process in Sb_2S_3 has been attributed to self-trapping in Sb_2S_3 due to local lattice distortions and considering the fact that the self-trapping will exist even in a perfect Sb_2S_3 crystal, the theoretical V_{oc} and PCE upper limits have been reduced from 1.4V to 0.8V and 28.6% to 16% respectively (Yang et al. 2019). Hence, as demonstrated by Yang et al. and Grad et al., the self-trapping phenomenon is inevitable in soft-1D Sb_2S_3 materials but can be minimized by stiffening the elastic properties of Sb_2S_3 in order to increase the PCE of Sb_2S_3 solar devices (Yang et al. 2019; Grad et al. 2021). On the other hand, as demonstrated by these investigations, self-trapping should also occur in Sb_2S_3 -sensitized photovoltaic devices in addition to extrinsic surface trapping. Further, Han, j. et. Al., in 2021 reported that the steady-state photoluminescence (PL) spectra of different Sb_2S_3 films deposited on quartz substrates and PL emission peaks locate at ca. 737 nm, which is close to the Sb_2S_3 absorption band edge shows lower PL intensity as a result of higher nonradiative recombination owing to the low crystallinity and relatively numerous trap states. Addition of $[\text{TMA}][\text{PF}_6]$, leads to strong PL intensities which is favorable for the crystallinity improvement and defect healing and the PCE efficiency increases from 4.27 to 6.63 (Han et al. 2021).

3 Theoretical study

Theoretical calculations have been used to explain and categorize the reason(s) for the reported low efficiencies for Sb_2S_3 -based solar cells, paving the way for future research into the impact of recombination mechanisms on solar cells at both the Sb_2S_3 bulk material and the Sb_2S_3 /buffer layer interface (Jiménez et al. 2018). According to theoretical calculations by Courel et al., the defects have an impact on minority carrier lifetime, buffer/absorber interface recombination, tunneling enhanced recombination, and recombination due to bulk defects as the major loss mechanisms for the device glass/Au/ Sb_2S_3 /CdS/ZnO/ZnO:Al configuration. (Courel et al. 2019) For their theoretical calculations, the diode ideality factor of 2 has been used as the observed experimental efficiencies are far behind the efficiency values predicted. Ideality factor 1 is taken under the diffusion and radiative recombination mechanisms (Courel et al. 2019).

By simulating each dominant loss mechanism in CdS/ Sb_2S_3 interface recombination, Sb_2S_3 non-radiative recombination, and tunneling enhanced recombination at Sb_2S_3

absorber material separately on V_{oc} , J_{sc} and FF (Courel et al. 2019), (table 2 in Courel et al. (2019)) recombination at Sb_2S_3 bulk material and CdS/Sb_2S_3 interface have been identified as the dominant loss mechanism (Courel et al. 2019). Furthermore, since the simulated solar cell parameters based on the defect loss mechanism agree well with the experimentally measured ones (PCE~5.0% and V_{oc} 600–700 mV), the major defects in Sb_2S_3 were reported to be the limiting factor for device performance. On the other hand, the 11.06% and 18.5% PCE obtained under non-optimized and ideal series/shunt resistance values respectively have mainly attributed to the change in FF from 53.9% (non-ideal conditions) to 83% (ideal conditions) implying that more efforts should be made to optimize series resistance (R_s), shunt resistance (R_{sh}) to overcome the efficiency barrier (Courel et al. 2019). Poor series and shunt resistances have been found to arise as a result of non-ideal band alignment, the formation of Schottky contacts, element diffusion, the formation of defects at the semiconductor/metal contact, and poor crystallinity (Fig. 4a).

By performing two-stage modeling for common buffer layers used in Sb_2S_3 -based solar cells, Islam et al. reported a similar loss mechanism and the critical roles of the R_s and R_{sh} as well as recombination effect for PEC performance (Fig. 4b, c, d) (Islam and Thakur 2020). In addition, it was noted that the optimum thickness of the Sb_2S_3 absorber layer (considering both electronic and optical properties), was highly dependent on the type of buffer layer used, with optimal thicknesses reported to be ~1.5–1.8 μm for Sb_2S_3/ZnS while for Sb_2S_3/CdS and Sb_2S_3/TiO_2 was found to be 2–4 μm . ZnS material is non-toxic compared to CdS material, and the quantum efficiency of thin-film solar cells with CdS buffer layer decline at short wavelengths due to the optical absorption losses from the CdS (Jeon et al. 2016). However, ZnS shows higher optimal transmittance about 95% in visible region (Agrawal et al. 2020). Typical thickness CdS window layer is about 30–80 nm and the less thickness of CdS layer may create pinholes and develop shunting path, leads to lower performance of solar cell (Agrawal et al. 2020). Furthermore, Islam et al. demonstrated the importance of proper band alignment and thus the conduction band offset (CBO) between the absorber and buffer layers for efficient charge flow across the junction to control interfacial recombination in their simulation work, and better PCE performances were predicted with ZnS buffer layers than with CdS (bandgap 2.4 eV) and TiO_2 buffer layers (bandgap 3.2 eV). As shown in Figs. 5a, b, and c, the CBO of ZnS, CdS, and TiO_2 are +0.26, -0.2, and -0.5 eV, respectively, and thus a spike-type CBO has been reported for ZnO, whereas a cliff-type CBO has been reported for CdS and TiO_2 , respectively, and thus, as shown in Fig. 5d and e, electron hole recombination is energetically favorable for cliff and for spike-type CBO having a small CBO i.e. less than +0.04 eV, mobility of holes is not favored

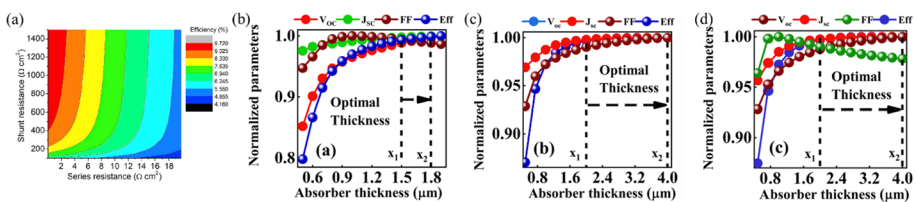


Fig. 4 a Sb_2S_3 solar cell efficiency as a function of series and shunt resistance values under non-optimized values of Sb_2S_3 minority carrier lifetime and Sb_2S_3/CdS interface recombination speed. Reproduced with permission, [42]; Effect of the thickness of the absorber layer on the performance parameters device for **b** Sb_2S_3/ZnS , **c** Sb_2S_3/CdS , and **d** Sb_2S_3/TiO_2 combination respectively. Reproduced with permission, Islam and Thakur (2020).

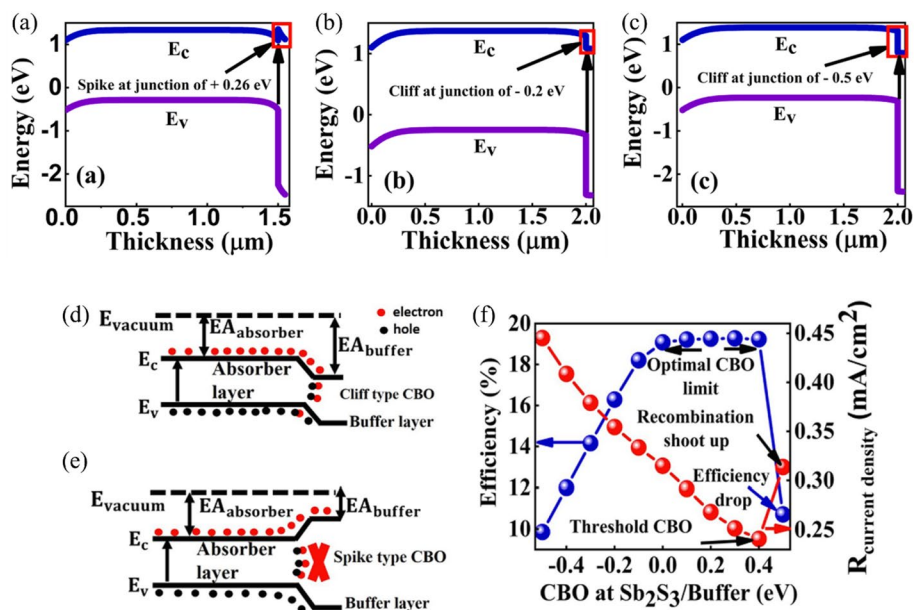


Fig. 5 The band diagram of the device structure and conduction band offset (CBO) at absorber/buffer counterpart interface. **a–c** represent device for $\text{Sb}_2\text{S}_3/\text{ZnS}$, $\text{Sb}_2\text{S}_3/\text{CdS}$ and $\text{Sb}_2\text{S}_3/\text{TiO}_2$ combination respectively. Reproduced with permission Islam and Thakur (2020). The schematic diagram of **d** the cliff and **e** spike type CBO at the absorber/buffer interface **d** shows that interfacial recombination is more favorable for cliff type junction and **e** shows that interfacial recombination is negligible for spike type junction. **f** Effect of CBO on the recombination current and efficiency of the solar device. Reproduced with permission Islam and Thakur (2020).

while photo-generated electrons can transfer via tunneling process. The spike -type energy level alignment is favorable for defeat the recombination due to the formation of the potential barrier at the interface but too positive CBO leads to high potential barrier at the interface and leads to lower short-circuit current and the solar cell performances (Wang et al. 2022). On the other hand, for efficient charge transfer from Sb_2S_3 to buffer layer, a cliff type CBO is preferred. The bulk defects in the materials and the interface should be optimized owing to the bulk defects act as a trap state leads to charge recombination. Further, based on their overall simulation work, as shown in Fig. 5a, b, c, d, e, f, the need for a spike-type band alignment at the front contact and a high work function metal at the back contact as essential requirements to improve device performance has been identified. Although, they did not consider the interface-modulated doping at the interface.

On the other hand, Cao et al. demonstrated the optimized parameters for each device component through the simulation of a one-dimensional device with an n-i-p planar heterojunction front contact/ETL/ Sb_2S_3 /HTL/back contact (Fig. 6a, b) (Cao et al. 2020). In the case of ETL, decreasing the CBM_{ETL} reported to decrease the potential barrier, and even Sb_2S_3 layer's energy band will bend downward, increasing the CBM_{ETL} beyond -4.0 eV facilitates the electron collection due to the decreased potential barrier, whereas decreasing the VBM_{HTL} reported to decrease the electric field, facilitating hole collection due to decreased potential barrier. As a result, Cao et al. predicted (Fig. 6b) that an efficient carrier transfer process for Sb_2S_3 as an absorber layer could be achieved by selecting an

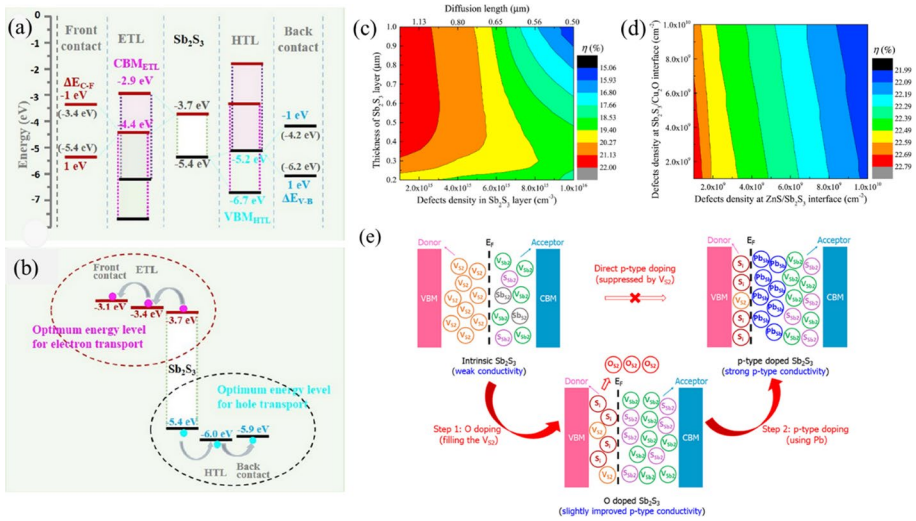


Fig. 6 **a** Schematic of energy-level diagram of Sb_2S_3 solar cell with a large parameter window for electron transport layers and hole transport layers. Reproduced with permission, Cao et al. (2020), **b** a typical energy level alignment with the optimal band structure of electron transport layer as well as the hole transport layer. Reproduced with permission, Cao et al. (2020), **c** The photovoltaic performance parameters (η) of the Sb_2S_3 solar cells with different values of interface defect density at $\text{ZnS}/\text{Sb}_2\text{S}_3$ and $\text{Sb}_2\text{S}_3/\text{Cu}_2\text{O}$ hetero-interfaces. Reproduced with permission, Xiao et al. (2020), **d** The photovoltaic performance parameters (η) of the Sb_2S_3 solar cells with different values of N_t (corresponding different LD) and thickness of Sb_2S_3 layer. Reproduced with permission, Xiao et al. (2020), **e** Schematic illustration of the strategy for efficient p-type doping in Sb_2S_3 . E_F in this figure means the Fermi level Reproduced with permission, Cai et al. (2020)

ETL with a conduction band minimum of $-4.4 \text{ eV} < \text{CBM} < -3.2 \text{ eV}$ and an HTL with a valence band maximum of $-5.2 \text{ eV} > \text{VBM} > -6.4 \text{ eV}$ owing to the interfacial potential barrier becoming negligible with appropriate energy levels of both ETL and HTL (Cao et al. 2020). Accordingly, the best PCE of the Sb_2S_3 cell with the CBM_{ETL} and VBM_{HTL} is suggested to be -3.5 eV and -6.1 eV , respectively.

By exploring the effect of the relative positions of the CBM_{ETL} vs. the work function of the front electrode as well as VBM_{HTL} Vs. the work function of the back contact, the electron and hole collection properties were predicted respectively by Cao et al. in the same study (Cao et al. 2020). Accordingly, a PCE of $\sim 14\%$ has been predicted with the CBM_{ETL} less than -3.4 eV , and $\Delta E_{\text{C-F}}$ ranging from -1 eV to 0.4 eV , while maintaining the detailed parameters nearly the same. Approximately the same performance has been reported for different VBM_{HTL} and $\Delta E_{\text{V-B}}$ values, until the $\Delta E_{\text{V-B}}$ is less than -0.6 eV . Within the range of the above parameters, when the CBM_{ETL} is -3.4 eV , $\Delta E_{\text{C-F}}$ is -0.3 eV , VBM_{HTL} is -6 eV and $\Delta E_{\text{V-B}}$ is -0.1 eV , a PCE of 15.62% ($V_{\text{oc}} = 1.125 \text{ V}$, $J_{\text{sc}} = 17.83 \text{ mA}/\text{cm}^2$, $\text{FF} = 77.91\%$) can be obtained (Cao et al. 2020).

However, Cao et al. has not considered carrier recombination completely in their simulation study, which is one of the major loss mechanisms in Sb_2S_3 solar cells due to various electrically active intrinsic point defects and extrinsic defects in Sb_2S_3 (Cao et al. 2020). Hence, Xiao et al., in their investigation, a numerical simulation has been done on full-inorganic $\text{FTO}/\text{ZnS}/\text{Sb}_2\text{S}_3/\text{HTLs}/\text{Au}$, solar cell considering different bulk defect densities in bulk Sb_2S_3 as well as $\text{ETL}/\text{Sb}_2\text{S}_3$ and $\text{Sb}_2\text{S}_3/\text{HTL}$ hetero-interfaces (Xiao et al. 2020).

The simulation results shown in Fig. 6c demonstrated the importance of having a proper higher carrier diffusion length than the thickness of the Sb_2S_3 layer to facilitate the conversion of photogenerated electron–hole pairs to photogenerated current, and it has been noted that the Sb_2S_3 layer thickness significantly affecting charge collection efficiency in high-defect density region corresponds to short carrier diffusion length. The highest device performance has been predicted at lower values of N_t (10^{15} cm^{-3}) and larger values of L_D (1.6 μm) for an average Sb_2S_3 thickness of 0.8 μm . On the other hand, it has been demonstrated that improving hetero-junction quality can improve device performance by maintaining a lower interface defect density of $\sim 10^9 \text{ cm}^{-2}$ at both $\text{ZnS}/\text{Sb}_2\text{S}_3$ and $\text{Sb}_2\text{S}_3/\text{Cu}_2\text{O}$ interfaces, which could be achieved by improving the hetero-junction quality (Fig. 6d).

Based on the calculated band structure and density of states for Sb_2S_3 , the conduction band minimum is composed mainly of the Sb 5p and S 3p orbitals an antibonding state of the p–p hybridization, and the VBM is composed mainly of the Sb 5 s and S 3p orbitals in the antibonding states of the s–p hybridization (Cai et al. 2020). The high electrical resistivity due to the presence of intrinsic point defects in Sb_2S_3 is a critical factor that causes the low efficiency and to address the relationship between the resistivity vs. the point defects in Sb_2S_3 . Cai et al., investigated how the intrinsic defect limits the electrical conductivity and a two-step p-Type doping strategy for overcoming the efficiency bottleneck of Sb_2S_3 -based solar cells was proposed (Cai et al. 2020). The formation energy of V_{S2} and V_{S3} are similar, and the formation energy of neutral V_{S1} is lower than that of V_{S2} and V_{S3} . When V_{S1} is ionized to +2 charge state, its formation energy becomes higher than that of V_{S2} and V_{S3} . For cation vacancies, V_{Sb1} and V_{Sb2} have similar formation energies. From the result of the first-principle calculation, Cai et al. reported that the high-resistivity that limit the performance of Sb_2S_3 results from the compensation between the intrinsic donor, V_S and acceptors V_{Sb} , S_b , and S_{Sb} formed due to their comparatively low formation energy pinning of the Fermi level at the middle of the band gap in intrinsic Sb_2S_3 . The increase in conductivity caused by external p-type doping in intrinsic Sb_2S_3 was discovered to produce more donor V_S sites, resulting in many electron carriers and pushing the Fermi level up, making p-type doping difficult to realize. Similarly, external n-type doping in Sb_2S_3 was also found to be difficult to be realized due to the formation of high concentration dominant intrinsic acceptor V_{Sb2} during external doping. Hence, Cai et al. proposed a two-step doping strategy that allows for the introduction of p-type dopants later (Cai et al. 2020). As shown in Fig. 6e, donor Vs defects were passivated first with O, then with p-type doping to increase hole carrier concentration and sulfurization of the O-doped Sb_2S_3 under the S-rich condition to suppress the other p-type limiting and recombination-center donor defects. During O passivation, O is discovered to occupy one (S2) of the two S sites, forming the OS2 defect, which is the main source of hole trap sites, and because OS2 has a low formation energy, the dominant donor VS2 is filled by O. As a result, the Fermi level is reduced to 0.58 eV above the valence band maximum (VBM), allowing the hole carrier concentration and p-type conductivity to increase. However, in the S-rich sulfurization process, S_i has been identified as the dominant defect, and the Fermi level has been set at approximately 0.58 eV above the VBM due to competition between the dominant donor Si and the dominant acceptor S_{Sb2} . As a result, after sulfurization, improved p-type conductivity with higher hole concentration has been predicted.

On the other hand, high resistivity that occurs due to pinning of the Fermi level near the mid-gap due to the presence of defects V_{Sb} and V_S at deep levels inside the band gap which can trap the charge free carriers in Sb_2S_3 were systematically investigated by using hybrid functional theory by (Zhao et al. 2021) Extrinsic dopants such as Zn, Cu, Ti, Br, and Cl, as well as their complexes with native defects, were also reported in the

same study to control carrier transport in Sb_2S_3 . Zhao et al. clearly demonstrated that Cl/Br and Zn/Cu dopants complexing with native defects can reduce the trapping energy of the native defects, improving carrier transport efficiency. A Cu_{Sb} acceptor can easily bind with a V_{S} donor, forming a neutral $\text{Cu}_{\text{Sb}} + \text{V}_{\text{S}}$ complex that is much more delocalized and difficult to dissociate, as shown in Fig. 7. The doped Cu metal in Sb_2S_3 films is primarily anchored with sulfur at the surface and grain boundaries, resulting in the formation of single-phase Sb_2S_3 up to 2% Cu-doping concentration and the emergence of a minor CuSbS_2 phase beyond 4% Cu-doping concentration (Lei et al. 2019; Chalapati et al. 2019). $\text{Cu}_{\text{Sb}2} + \text{V}_{\text{S}3}$ defect levels also become shallower than those of isolated defects due to donor-acceptor coupling, which pushes the electron and hole-trapping levels apart, resulting in the electronic trapping level being closer to the CBM and the hole-trapping level being closer to the VBM, as shown in Fig. 7. As a result, Zhao et al. demonstrated that Fermi level pinning can be eliminated by chemical doping of shallow donors with Cl, Br or shallow acceptors with Zn, Cu, resulting in a higher carrier density and a means to fine-tune the properties of the interface with other components of the solar cell such as the electron-extraction layer and the hole-transport layer. According to the simulation results, Zn and Cl were discovered to be the best dopants for reducing V_{Sb} and V_{S} defects, respectively, because Zn_{Sb} and Cl_{S} are much shallower than vacancies (V_{Sb} and V_{S}).

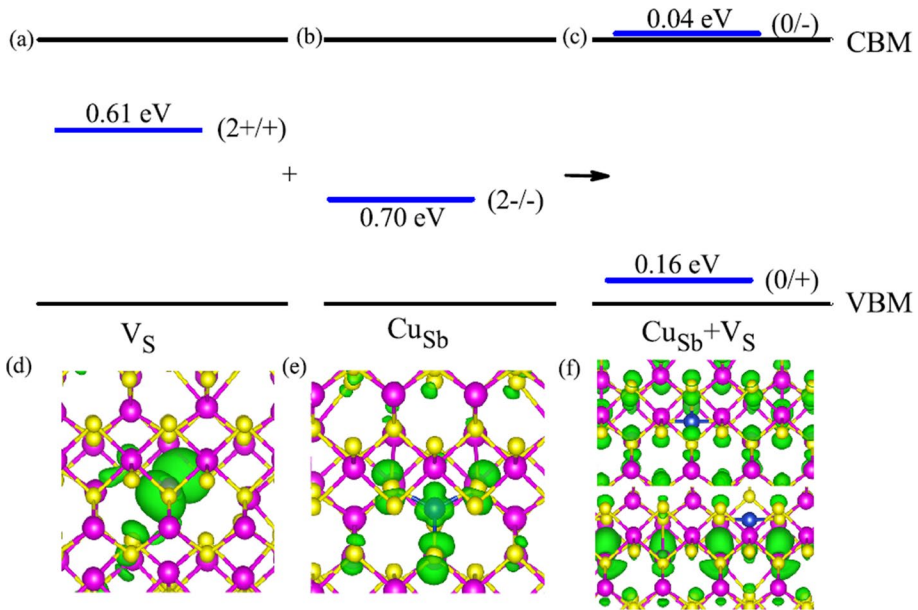


Fig. 7 Effects of $\text{Cu}_{\text{Sb}1}\text{-V}_{\text{S}1}$ binding on the electron-trapping level of $\text{V}_{\text{S}1}$ and the hole-trapping level of $\text{Cu}_{\text{Sb}1}$. **a** and **d** show the (2+/+) electron trapping level of $\text{V}_{\text{S}1}$ and the charge density of the trapped electron at $(\text{V}_{\text{S}1})^+$, respectively; **b** and **e** show the (2-/-) hole trapping level of $\text{Cu}_{\text{Sb}1}$ and the charge density of the trapped hole at $(\text{Cu}_{\text{Sb}1})^-$, respectively; (c) shows the (0/-) electron-trapping and the (+/0) hole-trapping levels of $\text{Cu}_{\text{Sb}1} + \text{V}_{\text{S}1}$; and (f) shows the trapped electron at $(\text{Cu}_{\text{Sb}1} + \text{V}_{\text{S}1})^-$ (upper panel) and the trapped hole at $(\text{Cu}_{\text{Sb}1} + \text{V}_{\text{S}1})^+$ (lower panel). Reproduced with permission, Zhao et al. (2021).

4 Prospective and summary—conclusions and outlook

This review includes a discussion of the limitations of Sb_2S_3 -based photovoltaic devices using theoretical and experimental study and to set the upper limit and overcome the efficiency barrier of Sb_2S_3 thin-film-based solar cells paving a new path to improving Sb_2S_3 performance in the future. In a recent review, it was shown how the morphology and structural changes in Sb_2S_3 thin-films produced using various fabrication techniques and conditions affect solar cell performance (Farhana et al. 2023). It has been noted the formation of finite $(\text{Sb}_4\text{S}_6)_n$ ribbon-like structures along the c-axis are common in orthorhombic Sb_2S_3 and the bandgap of Sb_2S_3 reported to vary between 1.56 and 2.25 eV, while the reported conductivity of Sb_2S_3 in room temperature ranges between 10^{-8} and $10^{-9} \Omega^{-1} \text{cm}^{-1}$ depending on the fabrication methods and parameters. The most common factors that have been attributed to the reported poor performance of Sb_2S_3 in solar devices fabricated by different methods are intrinsically formed traps and the presence of surface defect states. The types of defects in Sb_2S_3 and their binding energies and positions within the forbidden region have been explained by DLTS and theoretical investigations (Farhana et al. 2023). The reported poor performance of Sb_2S_3 in solar devices implies that significant factors such as intrinsically formed traps and the presence of surface defect states, which have been identified as limiting factors for device performance, have not been successfully addressed. As a result, achieving the goal of a 28% efficient Sb_2S_3 solar cell is a significant challenge due to the large gap between the theoretical predicted and current record Sb_2S_3 device PCE, which necessitates a large number of comprehensive research efforts. However, the lack of such coordinated studies could be one of the reasons for the slow progress on Sb_2S_3 solar cells.

Experimentally it has been shown that major donor defects or electron traps, Sb-S-vacancy (V_S), and Sb-antisite, (Sb_S), appearing in Sb-rich Sb_2S_3 act as carrier traps/recombination sites, resulting in electron quasi-Fermi level pinning due to inefficient extraction of trapped photo-excited carriers, whereas acceptor defects or hole traps Sb-vacancy (V_{Sb}) and S-antisite (S_{Sb}) for the S-rich film which also acts as carrier traps/recombination sites, the Fermi level pinning effects lessen and hence improved V_{OC} can be expected. Hence, investigating the S-rich Sb_2S_3 film for the next efficiency breakthrough is worthwhile. However, even with the preferred [hk1] crystalline orientation in Sb_2S_3 , which could benefit carrier transport, Sb_2S_3 has low carrier mobility due to high bulk resistance and poor carrier collection efficiency. Furthermore, more research should be focused on designing a built-in electric field with a fully depleted absorber layer to alleviate the constraints of fill factor and carrier collection efficiency of Sb_2S_3 solar cells caused by low carrier mobility. As a result, a p-i-n planar or sensitized structure with a fully depleted absorber, allowing the built-in electric field to be applied to the entire absorber layer, would result in increased carrier transport efficiency and, as a result, increased power conversion efficiency. The major energy loss process in Sb_2S_3 has been attributed to the low charge carrier mobility due to the intrinsically self-trapping of photoexcited carriers in Sb_2S_3 by lattice deformation, as demonstrated by (Yang et al. 2019; Grad et al. 2021). The "self-trapping phenomenon" in soft-1D Sb_2S_3 materials is unavoidable, but it can only be minimized by stiffening the elastic properties of Sb_2S_3 to increase the PCE of Sb_2S_3 solar devices. As a result, it is critical to look for novel ways to overcome the self-trapping phenomenon in Sb_2S_3 materials in order to break through the current PCE limits.

According to the simulation results, the major defects in Sb_2S_3 are the limiting factor for device performance. The simulation of PCE and series/shunt resistance of Sb_2S_3

film, on the other hand, revealed improved FF under optimized series/shunt resistance, implying that more efforts should be made to optimize R_s and R_{sh} to overcome the efficiency barrier. Poor series and shunt resistances have been found to arise as a result of non-ideal band alignment, the formation of Schottky contacts, element diffusion, and the formation of defects at the semiconductor/metal contact, so these parameters should be considered when optimizing Sb_2S_3 solar cell performance. Another factor one should pay attention is the proper selection of ETL and HTL, as simulation results indicated that an efficient carrier transfer process could be achieved for Sb_2S_3 with an ETL with a conduction band minimum of $-4.4 \text{ eV} < CBM_{ETL} < -3.2 \text{ eV}$ and an HTL with a valence band maximum of $-5.2 \text{ eV} > VBM_{HTL} > -6.4 \text{ eV}$ owing to the interfacial potential barrier become negligible with appropriate energy levels of both ETL and HTL. By exploring the effect of the relative positions of the CBM_{ETL} vs. the work function of the front electrode as well as VBM_{HTL} Vs. the work function of the back contact, a PCE of 15.62% ($V_{oc}=1.125 \text{ V}$, $J_{sc}=17.83 \text{ mA/cm}^2$, $FF=77.91\%$) has been projected when the CBM_{ETL} is -3.4 eV , ΔE_{C-F} is -0.3 eV , VBM_{HTL} is -6 eV and ΔE_{V-B} is -0.1 eV . As it has been suggested the best PCE of the Sb_2S_3 cell with the CBM_{ETL} and VBM_{HTL} at -3.5 eV and -6.1 eV respectively, it is worthy to investigate different suitable ETL and HTL in order to break the efficiency barrier. For an average Sb_2S_3 thickness of $0.8 \mu\text{m}$, the highest device performance has been predicted at lower values of N_t (10^{15} cm^{-3}) and larger values of L_D ($1.6 \mu\text{m}$). On the other hand, it has been demonstrated that hetero-junction quality can improve device performance by maintaining a lower interface defect density of $\sim 10^9 \text{ cm}^{-2}$ at both ZnS/ Sb_2S_3 and Sb_2S_3/Cu_2O interfaces. On the other hand, it has been demonstrated the difficulty of conductivity increase through external p-type doping in intrinsic Sb_2S_3 as it may lead to producing more donor V_s sites, consequently producing many electron carriers and pushing the Fermi level up, and thus make the p-type doping difficult to be realized by external doping. Hence, as suggested by Cai et al., attempts should be done to increase the p-type doping by a two-step doping strategy (Cai et al. 2020). Hence a proper experiment should be carried out to increase the p-type conductivity by passivating the Sb_2S_3 Vs defects first by using O under the S-rich condition to increase the hole carrier concentration and suppress the other p-type limiting and recombination-center donor defects, and later by introducing different external p-type dopants such as Pb, to further increase its p-type conductivity to overcome the current efficiency bottleneck of Sb_2S_3 -based solar cells.

Finally, given the recent interest in the theoretical and experimental investigation of excited-state carrier dynamics and defect properties in Sb_2S_3 , concerted optimization of Sb_2S_3 -based solar cell based on theoretically predicted parameters may lead to a better understanding of the different recombination losses in both Sb_2S_3 bulk and interfaces of Sb_2S_3/ETL and Sb_2S_3/HTL could lead to promoting device performance (Cai et al. 2020; Courel et al. 2019; Cao et al. 2020; Xiao et al. 2020; Islam and Thakur 2020; Yang et al. 2019; Grad et al. 2021; Lian et al. 2021; Li et al. 2021).

5 Conclusion

Despite reported higher efficiencies for sensitized Sb_2S_3 Solar cells, the planar device structure is more competitive for Sb_2S_3 -based solar cells. The high density of interface defects and poor carrier transport are the limitation of Sb_2S_3 based solar cells. The major defects V_{sb} and V_s in Sb_2S_3 can be mitigated by doping with Zn/Cu and Br/Cl leading to increase charge carrier density and electron transport properties. A proper selection of the

buffer layer is important for efficient charge collection and to reduce the charge recombination. The major energy loss process in Sb_2S_3 is due to the "self-trapping phenomenon" in soft-1D Sb_2S_3 caused by lattice deformation, which cannot be totally unavoidable but can only be minimized by stiffening the elastic properties of Sb_2S_3 . Hence, it is critical to look for novel ways to overcome the self-trapping phenomenon in Sb_2S_3 materials in order to break through the current PCE limits. This review could lead to the utilization of earth-abundant and harmless Sb_2S_3 in the future.

Authors' contribution JB contributed to the study conception and design. Material preparation, data collection and analysis were performed by MAF, AM, HT, C-FY and JB. The manuscript was written through contributions of all authors. All authors have given approval to the final version of the manuscript.

Funding JB is thankful to Chinese Academy of Sciences for providing him a PIFI fellowship (2017VCA0003) to conduct this research. Financial supports from STS Regional Key Project of Chinese Academy of Sciences (KFJ-STC-QYZD-2021-02-003), Guangzhou Key Area R&D Program of Science and Technology Plan Project (202103040002, 202206050003), and Strategic Priority Research Program of the Chinese Academy of Sciences (XDA21070605) are highly appreciated. Funding from National Research Council, Sri Lanka, NRC-18-005 is highly appreciated.

Data availability Not applicable.

Declarations

Conflict of interest The authors have no relevant financial or non-financial interests to disclose.

Ethical approval Not applicable.

References

- Agrawal, D., Suthar, D., Agarwal, R., Himanshu, S.L., Patel, M.S.D.: Achieving desired quality of ZnS buffer layer by optimization using air annealing for solar cell applications. *Phys. Lett. A* **384**, 126557–126563 (2020). <https://doi.org/10.1016/j.physleta.2020.126557>
- Akilavasan, J., Wijeratne, K., Moutinho, H., Al-Jassim, M., Alamoud, A.R.M., Rajapakse, R.M.G., Bandara, J.: Hydrothermally synthesized titania nanotubes as a promising electron transport medium in dye sensitized solar cells exhibiting a record efficiency of 7.6% for 1-D based devices. *J. Mater. Chem. A* **1**, 5377–5385 (2013). <https://doi.org/10.1039/C3TA01576A>
- Aliyar Farhana, M., Bandara, J.: Enhancement of the photoconversion efficiency of Sb_2S_3 based solar cell by overall optimization of electron transport, light harvesting and hole transport layers. *Sol. Energy* **247**, 32–40 (2022). <https://doi.org/10.1016/j.solener.2022.10.025>
- Araújo, M., Lucas, F., Mascaro, L.: Effect of the electrodeposition potential on the photoelectroactivity of the $\text{SnS}/\text{Sb}_2\text{S}_3$ thin films. *J. Solid State Electrochem.* **24**, 389–399 (2020). <https://doi.org/10.1007/s10008-020-04508-2>
- Ben Nasr, T., Maghraoui-Meherzi, H., Ben Abdallah, H., Bennaceur, R.: Electronic structure and optical properties of Sb_2S_3 crystal. *Physica B* **406**, 287–292 (2011). <https://doi.org/10.1016/j.physb.2010.10.070>
- Boix, P.P., Lee, Y.H., Fabregat-Santiago, F., Im, S.H., Mora-Sero, I., Bisquert, J., Seok, S.I.: From flat to nanostructured photovoltaics: balance between thickness of the absorber and charge screening in sensitized solar cells. *ACS Nano* **6**, 873–880 (2011a)
- Boix, P.P., Larramona, G., Jacob, A., Delatouche, B., Mora-Seró, I., Bisquert, J.: Hole transport and recombination in all-solid Sb_2S_3 -sensitized TiO_2 solar cells using CuSCN as hole transporter. *J. Phys. Chem. C* **116**, 1579–1587 (2011b)
- Bosio, A., Pasini, S., Romeo, N.: The history of photovoltaics with emphasis on CdTe solar cells and modules. *Coatings* **10**, 344–374 (2020)

- Cai, Z., Dai, C.-M., Chen, S.: Intrinsic defect limit to the electrical conductivity and a two-step p-type doping strategy for overcoming the efficiency bottleneck of Sb_2S_3 -based solar cells. *J Solar RRL* **4**, 1900503–1900513 (2020)
- Cao, Y., Zhu, X., Jiang, J., Liu, C., Zhou, J., Ni, J., Zhang, J., Pang, J.: Rotational design of charge carrier transport layers for optimal antimony trisulfide solar cells and its integration in tandem devices. *J. Solar Energy Mater. Solar Cells* **206**, 110279–110289 (2020)
- Catchpole, K.R., Polman, A.: Plasmonic solar cells. *Opt. Express* **16**, 21793–21800 (2008). <https://doi.org/10.1364/OE.16.021793>
- Chalapathi, U., Poonaprakash, B., Park, S.: The effect of Cu-doping on the structural, microstructural, optical, and electrical properties of Sb_2S_3 thin films. *Chalcogenide Lett.* **16**, 449–455 (2019)
- Chang, J.A., Rhee, J.H., Im, S.H., Lee, Y.H., Kim, H.-J., Seok, S.I., Nazeeruddin, M.K., Gratzel, M.: High-Performance Nanostructured Inorganic–Organic Heterojunction Solar Cells. *Nano Lett.* **10**, 2609–2612 (2010). <https://doi.org/10.1021/nl101322h>
- Chang, Y., Lee, J., Yoon, H.: Alternative projection of the world energy consumption-in comparison with the 2010 international energy outlook. *Energy Policy* **50**, 154–160 (2012). <https://doi.org/10.1016/j.enpol.2012.07.059>
- Chen, C., Tang, J.: Open-circuit voltage loss of antimony chalcogenide solar cells: status, origin, and possible solutions. *ACS Energy Lett.* **5**, 2294–2304 (2020)
- Choi, Y.C., Lee, D.U., Noh, J.H., Kim, E.K., Seok, S.I.: Highly improved Sb_2S_3 sensitized-inorganic–organic heterojunction solar cells and quantification of traps by deep-level transient spectroscopy. *Adv. Func. Mater.* **24**, 3587–3592 (2014a). <https://doi.org/10.1002/adfm.201304238>
- Choi, Y.C., Lee, Y.H., Im, S.H., Noh, J.H., Mandal, T.N., Yang, W.S., Seok, S.I.: Efficient inorganic-organic heterojunction solar cells employing $\text{Sb}_2(\text{S}_x\text{Se}_{1-x})_3$ graded-composition sensitizers. *Adv. Energy Mater.* **4**, 1301680–1301685 (2014b)
- Christians, J.A., Kamat, P.V.: Trap and transfer. two-step hole injection across the $\text{Sb}_2\text{S}_3/\text{CuSCN}$ interface in solid-state solar cells. *ACS Nano* **7**, 7967–7974 (2013). <https://doi.org/10.1021/nn403058f>
- Christians, J.A., Leighton, D.T., Kamat, P.V.: Rate limiting interfacial hole transfer in Sb_2S_3 solid-state solar cells. *Energy Environ. Sci.* **7**, 1148–1158 (2014). <https://doi.org/10.1039/C3EE43844A>
- Courel, M., Jiménez, T., Arce-Plaza, A., Seuret-Jimenez, D., Morán-Lázaro, J.P., Sanchez, F.: A theoretical study on Sb_2S_3 solar cells: the path to overcome the efficiency barrier of 8%. *Solar Energy Mater. and Solar Cells* **201**, 110123–110134 (2019). <https://doi.org/10.1016/j.solmat.2019.110123>
- Dematage, N., Premalal, E., Konno, A.: Employment of CuI on Sb_2S_3 extremely thin absorber solar cell: N719 molecules as a dual role of a recombination blocking agent and an efficient hole shuttle. *Int. J. Electrochem. Sci.* **9**, 1729–1737 (2014)
- Eensalu, J.S., Katerski, A., Kärber, E., Acik, I.O., Mere, A., Krunks, M.: Uniform Sb_2S_3 optical coatings by chemical spray method. *Beilstein J. Nanotechnol.* **10**, 198–210 (2019)
- Ellingson, R.J., Beard, M.C., Johnson, J.C., Yu, P., Micic, O.I., Nozik, A.J., Shabaev, A., Efron, A.L.: Highly efficient multiple exciton generation in colloidal PbSe and PbS quantum dots. *Nano Lett.* **5**, 865–871 (2005). <https://doi.org/10.1021/nl0502672>
- Farhana, M.A., Manjiveevan, A., Bandara, J.: Recent advances and new research trends in Sb_2S_3 thin film based solar cells. *J. Sci.: Adv. Mater. Dev.* **8**, 100533–100558 (2023). <https://doi.org/10.1016/j.jsamd.2023.100533>
- Giordano, F., Abate, A., Correa Baena, J.P., Saliba, M., Matsui, T., Im, S.H., Zakeeruddin, S.M., Nazeeruddin, M.K., Hagfeldt, A., Graetzel, M.: Enhanced electronic properties in mesoporous TiO_2 with lithium doping for high-efficiency perovskite solar cells. *Nat. Commun.* **7**, 10379–10385 (2016). <https://doi.org/10.1038/ncomms10379>
- Gloeckler, M., Sankin, I., Zhao, Z.: CdTe solar cells at the threshold to 20% efficiency. *IEEE J. Photovolt.* **3**, 1389–1393 (2013)
- Grad, L., von Rohr, F.O., Hengsberger, M., Osterwalder, J.: Charge carrier dynamics and self-trapping on Sb_2S_3 (100). *J Phys. Rev. Mater.* **5**, 075401–075409 (2021)
- Guo, L., Zhang, B., Li, S., Zhang, Q., Buettner, M., Li, L., Qian, X., Yan, F.: Scalable and efficient Sb_2S_3 thin-film solar cells fabricated by close space sublimation. *APL Mater.* **7**, 041105–041111 (2019). <https://doi.org/10.1063/1.5090773>
- Han, J., Wang, S., Yang, J., Guo, S., Cao, Q., Tang, H., Pu, X., Gao, B., Li, X.: Solution-processed Sb_2S_3 planar thin film solar cells with a conversion efficiency of 6.9% at an open circuit voltage of 0.7 V achieved via surface passivation by a SbCl_3 interface layer. *ACS Appl. Mater. Interfaces* **12**, 4970–4979 (2020). <https://doi.org/10.1021/acsami.9b15148>
- Han, J., Pu, X., Zhou, H., Cao, Q., Wang, S., Yang, J., Zhao, J., Li, X.: Multidentate anchoring through additive engineering for highly efficient Sb_2S_3 planar thin film solar cells. *J. Mater. Sci. Technol.* **89**, 36–44 (2021). <https://doi.org/10.1016/j.jmst.2021.01.078>

- Hirai, Y., Kurokawa, Y., Yamada, A.: Numerical study of Cu(In, Ga)Se₂ solar cell performance toward 23% conversion efficiency. *Jpn. J. Appl. Phys.* **53**, 012301–012307 (2013). <https://doi.org/10.7567/jjap.53.012301>
- Hong, J.-Y., Lin, L.-Y., Li, X.: Electrodeposition of Sb₂S₃ light absorbers on TiO₂ nanorod array as photocatalyst for water oxidation. *Thin Solid Films* **651**, 124–130 (2018). <https://doi.org/10.1016/j.tsf.2018.02.038>
- Hsieh, Y.-D., Lee, M.-W., Wang, G.-J.: Sb₂S₃ quantum-dot sensitized solar cells with silicon nanowire photoelectrode. *Int. J. Photoenergy* **2015**, 213858–213868 (2015). <https://doi.org/10.1155/2015/213858>
- Islam, M.T., Thakur, A.K.: Two stage modelling of solar photovoltaic cells based on Sb₂S₃ absorber with three distinct buffer combinations. *Sol. Energy* **202**, 304–315 (2020). <https://doi.org/10.1016/j.solener.2020.03.058>
- Jeon, D.H., Hwang, D.K., Kim, D.H., Kang, J.K., Lee, C.S.: Nanotechnology optimization of the ZnS buffer layer by chemical bath deposition for Cu (In, Ga) Se₂ solar cells. *J. Nanosci. Nanotechnol.* **16**, 5398–5402 (2016)
- Jiménez, T., Seuret-Jiménez, D., Vigil-Galán, O., Basurto-Pensado, M.A., Courel, M.: Sb₂(S_{1-x}Se_x)₃ solar cells: the impact of radiative and non-radiative loss mechanisms. *J. Phys. d: Appl. Phys.* **51**, 435501–435513 (2018). <https://doi.org/10.1088/1361-6463/aaad6a>
- Kim, K.P., Hwang, D.K., Woo, S.H., Kim, D.H.: Fabrication of Sb₂S₃ hybrid solar cells based on embedded photoelectrodes of Ag nanowires-Au nanoparticles composite. *J. Nanosci. Nanotechnol.* **18**, 6520–6523 (2018). <https://doi.org/10.1166/jnn.2018.15677>
- Koc, H., Mamedov, A.M., Deligoz, E., Ozisik, H.: First principles prediction of the elastic, electronic, and optical properties of Sb₂S₃ and Sb₂Se₃ compounds. *Solid State Sci.* **14**, 1211–1220 (2012). <https://doi.org/10.1016/j.solidstatesciences.2012.06.003>
- Kondrotas, R., Chen, C., Tang, J.: Sb₂S₃ solar cells. *Joule* **2**, 857–878 (2018). <https://doi.org/10.1016/j.joule.2018.04.003>
- Kriisa, M., Krunks, M., Oja Acik, I., Kärber, E., Mikli, V.: The effect of tartaric acid in the deposition of Sb₂S₃ films by chemical spray pyrolysis. *Mater. Sci. Semicond. Process.* **40**, 867–872 (2015). <https://doi.org/10.1016/j.mssp.2015.07.049>
- Kumar, A., Kumar, D.: Numerical simulation of Sb₂S₃ based photovoltaic cell. *J. Eur. J. Mol. Clin. Med.* **7**, 3868–3872 (2020)
- Landau, L.J.P.Z.S.: Über die bewegung der elektronen in kristallgitter. *Phys. z. Sowjetunion* **3**, 664–645 (1933)
- Lee, D.U., Pak, S.W., Cho, S.G., Kim, E.K., Seok, S.I.: Defect states in hybrid solar cells consisting of Sb₂S₃ quantum dots and TiO₂ nanoparticles. *Appl. Phys. Lett.* **103**, 023901–023906 (2013). <https://doi.org/10.1063/1.4813272>
- Lei, H., Lin, T., Wang, X., Dai, P., Guo, Y., Gao, Y., Hou, D., Chen, J., Tan, Z.: Copper doping of Sb₂S₃: fabrication, properties, and photovoltaic application. *J. Mater. Sci.: Mater. Electr.* **30**, 21106–21116 (2019)
- Lewis, N.S., Crabtree, G., Nozik, A.J., Wasielewski, M.R., Alivisatos, P., Kung, H., Tsao, J., Chandler, E., Walukiewicz, W., Spittler, M., Ellingson, R., Overend, R., Mazer, J., Gress, M., Horwitz, J., Ashton, C., Herndon, B., Shapard, L., Nault, R.M.: Basic Research Needs for Solar Energy Utilization. Report of the Basic Energy Sciences Workshop on Solar Energy Utilization, (2005). <https://doi.org/10.2172/899136>
- Li, J., Huang, J., Li, K., Zeng, Y., Zhang, Y., Sun, K., Yan, C., Xue, C., Chen, C., Chen, T., Green, M.A., Tang, J., Hao, X.: Defect-resolved effective majority carrier mobility in highly anisotropic antimony chalcogenide thin-film solar cells. *J. Solar RRL* **5**, 2000693–2000700 (2021)
- Lian, W., Jiang, C., Yin, Y., Tang, R., Li, G., Zhang, L., Che, B., Chen, T.: Revealing composition and structure dependent deep-level defect in antimony trisulfide photovoltaics. *Nat. Commun.* **12**, 3260–3267 (2021). <https://doi.org/10.1038/s41467-021-23592-0>
- Liang, Y., Zhong, X., Song, H., Zhang, Y., Zhang, D., Zhang, Y., Wang, J.: Study of photovoltaic performance of Sb₂S₃/CdS quantum dot co-sensitized solar cells fabricated using iodine-based gel polymer electrolytes. *Appl. Phys. A* **124**, 1–8 (2018). <https://doi.org/10.1007/s00339-018-1953-2>
- Mahuli, N., Halder, D., Paul, A., Sarkar, S.K.: Atomic layer deposition of amorphous antimony sulfide (a-Sb₂S₃) as semiconductor sensitizer in extremely thin absorber solar cell. *J. Vacuum Sci. Technol. A* **38**, 032407–032419 (2020). <https://doi.org/10.1116/6.0000031>
- Manjeevan, A., Bandara, J.: Robust surface passivation of trap sites in PbS q-dots by controlling the thickness of CdS layers in PbS/CdS quantum dot solar cells. *Sol. Energy Mater. Sol. Cells* **147**, 157–163 (2016). <https://doi.org/10.1016/j.solmat.2015.12.014>

- Myagmarsereejid, P., Ingram, M., Batmunkh, M., Zhong, Y.L.: Doping strategies in Sb_2S_3 thin films for solar cells. *Small* **17**, 2100241–2100258 (2021). <https://doi.org/10.1002/sml.202100241>
- Pastuszak, J., Węgierek, P.: Photovoltaic cell generations and current research directions for their development. *Materials (basel Switzerland)* **15**, 5542–5572 (2022). <https://doi.org/10.3390/ma15165542>
- Radzwan, A., Ahmed, R., Shaari, A., Lawal, A., Ng, Y.X.: First-principles calculations of antimony sulphide Sb_2S_3 . *Malays. J. Fundam. Appl. Sci.* **13**, 285–289 (2017). <https://doi.org/10.1113/mjfas.v13n3.598>
- Shang, M., Zhang, J., Wei, S., Zhu, Y., Wang, L., Hou, H., Fujikawa, T., Ueno, N., Wu, Y.: Bi doped Sb_2S_3 for low effective mass and optimized optical property. *J. Mater. Chem. C* **4**, 5081–5090 (2016). <https://doi.org/10.1039/C6TC00513F>
- Sun, Z., Peng, Z., Liu, Z., Chen, J., Li, W., Qiu, W., Chen, J.: Band energy modulation on Cu-doped Sb_2S_3 -based photoelectrodes for charge generation and transfer property of quantum dot-sensitized solar cells. *J. Nanopart. Res.* **22**, 282–291 (2020). <https://doi.org/10.1007/s11051-020-05009-z>
- Suryawanshi, M., Agawane, G., Bhosale, S., Shin, S., Patil, P., Kim, J., Moholkar, A.: CZTS based thin film solar cells: a status review. *Mater. Technol.* **28**, 98–109 (2013). <https://doi.org/10.1179/1753555712Y.0000000038>
- Todorov, T.K., Tang, J., Bag, S., Gunawan, O., Gokmen, T., Zhu, Y., Mitzi, D.B.: Beyond 11% Efficiency: characteristics of state-of-the-art $\text{Cu}_2\text{ZnSn(S, Se)}_4$ solar cells. *Adv. Energy Mater.* **3**, 34–38 (2013). <https://doi.org/10.1002/aenm.201200348>
- Wang, Y.-C., Zeng, Y.-Y., Li, L.-H., Qin, C., Wang, Y.-W., Lou, Z.-R., Liu, F.-Y., Ye, Z.-Z., Zhu, L.-P.: A stable and efficient photocathode using an Sb_2S_3 absorber in a near-neutral electrolyte for water splitting. *ACS Appl. Energy Mater.* **3**, 6188–6194 (2020). <https://doi.org/10.1021/acsaeam.0c00210>
- Wang, Y., Ji, S., Shin, B.: Interface engineering of antimony selenide solar cells: a review on the optimization of energy band alignments. *J. Phys.: Energy* **4**, 044002–044020 (2022). <https://doi.org/10.1088/2515-7655/ac8578>
- Xiao, Y., Wang, H., Kuang, H.: Numerical simulation and performance optimization of Sb_2S_3 solar cell with a hole transport layer. *J. Opt. Mater.* **108**, 110414–110424 (2020)
- Yang, Z., Wang, X., Chen, Y., Zheng, Z., Chen, Z., Xu, W., Liu, W., Yang, Y., Zhao, J., Chen, T., Zhu, H.: Ultrafast self-trapping of photoexcited carriers sets the upper limit on antimony trisulfide photovoltaic devices. *Nat. Commun.* **10**, 4540–4548 (2019). <https://doi.org/10.1038/s41467-019-12445-6>
- Zeng, K., Xue, D.-J., Tang, J.: Antimony selenide thin-film solar cells. *Semicond. Sci. Technol.* **31**, 063001–063014 (2016)
- Zeng, Y., Sun, K., Huang, J., Nielsen, M.P., Ji, F., Sha, C., Yuan, S., Zhang, X., Yan, C., Liu, X.: Quasi-vertically-orientated antimony sulfide inorganic thin-film solar cells achieved by vapor transport deposition. *ACS Appl. Mater. Interfaces* **12**, 22825–22834 (2020)
- Zhang, Y., Li, S.A., Tang, R., Wang, X., Chen, C., Lian, W., Chen, T.: Phosphotungstic acid regulated chemical bath deposition of Sb_2S_3 for high-efficiency planar heterojunction solar cell. *Energy Technol.* **6**, 2126–2131 (2018). <https://doi.org/10.1002/ente.201800238>
- Zhao, R., Yang, X., Shi, H., Du, M.-H.: Intrinsic and complex defect engineering of quasi-one-dimensional ribbons Sb_2S_3 for photovoltaics performance. *Phys. Rev. Mater.* **5**, 054605–054611 (2021). <https://doi.org/10.1103/PhysRevMaterials.5.054605>
- Zhong, J., Zhang, X., Zheng, Y., Zheng, M., Wen, M., Wu, S., Gao, J., Gao, X., Liu, J.-M., Zhao, H.: High efficiency solar cells as fabricated by Sb_2S_3 -modified TiO_2 nanofibrous networks. *ACS Appl. Mater. Interfaces* **5**, 8345–8350 (2013)
- Zhou, Y., Wang, L., Chen, S., Qin, S., Liu, X., Chen, J., Xue, D.-J., Luo, M., Cao, Y., Cheng, Y.: Thin-film Sb_2Se_3 photovoltaics with oriented one-dimensional ribbons and benign grain boundaries. *J. Nat. Photonics* **9**, 409–415 (2015)
- Zhou, Z., Xu, S., Song, J., Jin, Y., Yue, Q., Qian, Y., Liu, F., Zhang, F., Zhu, X.: High-efficiency small-molecule ternary solar cells with a hierarchical morphology enabled by synergizing fullerene and non-fullerene acceptors. *Nat. Energy* **3**, 952–959 (2018). <https://doi.org/10.1038/s41560-018-0234-9>
- Zimmermann, E., Pfadler, T., Kalb, J., Dorman, J.A., Sommer, D., Hahn, G., Weickert, J., Schmidt-Mende, L.: Toward high-efficiency solution-processed planar heterojunction Sb_2S_3 solar cells. *Adv. Sci.* **2**, 1500059–1500066 (2015)

Publisher's Note Springer Nature remains neutral with regard to jurisdictional claims in published maps and institutional affiliations.

Springer Nature or its licensor (e.g. a society or other partner) holds exclusive rights to this article under a publishing agreement with the author(s) or other rightsholder(s); author self-archiving of the accepted manuscript version of this article is solely governed by the terms of such publishing agreement and applicable law.

Terms and Conditions

Springer Nature journal content, brought to you courtesy of Springer Nature Customer Service Center GmbH (“Springer Nature”).

Springer Nature supports a reasonable amount of sharing of research papers by authors, subscribers and authorised users (“Users”), for small-scale personal, non-commercial use provided that all copyright, trade and service marks and other proprietary notices are maintained. By accessing, sharing, receiving or otherwise using the Springer Nature journal content you agree to these terms of use (“Terms”). For these purposes, Springer Nature considers academic use (by researchers and students) to be non-commercial.

These Terms are supplementary and will apply in addition to any applicable website terms and conditions, a relevant site licence or a personal subscription. These Terms will prevail over any conflict or ambiguity with regards to the relevant terms, a site licence or a personal subscription (to the extent of the conflict or ambiguity only). For Creative Commons-licensed articles, the terms of the Creative Commons license used will apply.

We collect and use personal data to provide access to the Springer Nature journal content. We may also use these personal data internally within ResearchGate and Springer Nature and as agreed share it, in an anonymised way, for purposes of tracking, analysis and reporting. We will not otherwise disclose your personal data outside the ResearchGate or the Springer Nature group of companies unless we have your permission as detailed in the Privacy Policy.

While Users may use the Springer Nature journal content for small scale, personal non-commercial use, it is important to note that Users may not:

1. use such content for the purpose of providing other users with access on a regular or large scale basis or as a means to circumvent access control;
2. use such content where to do so would be considered a criminal or statutory offence in any jurisdiction, or gives rise to civil liability, or is otherwise unlawful;
3. falsely or misleadingly imply or suggest endorsement, approval, sponsorship, or association unless explicitly agreed to by Springer Nature in writing;
4. use bots or other automated methods to access the content or redirect messages
5. override any security feature or exclusionary protocol; or
6. share the content in order to create substitute for Springer Nature products or services or a systematic database of Springer Nature journal content.

In line with the restriction against commercial use, Springer Nature does not permit the creation of a product or service that creates revenue, royalties, rent or income from our content or its inclusion as part of a paid for service or for other commercial gain. Springer Nature journal content cannot be used for inter-library loans and librarians may not upload Springer Nature journal content on a large scale into their, or any other, institutional repository.

These terms of use are reviewed regularly and may be amended at any time. Springer Nature is not obligated to publish any information or content on this website and may remove it or features or functionality at our sole discretion, at any time with or without notice. Springer Nature may revoke this licence to you at any time and remove access to any copies of the Springer Nature journal content which have been saved.

To the fullest extent permitted by law, Springer Nature makes no warranties, representations or guarantees to Users, either express or implied with respect to the Springer nature journal content and all parties disclaim and waive any implied warranties or warranties imposed by law, including merchantability or fitness for any particular purpose.

Please note that these rights do not automatically extend to content, data or other material published by Springer Nature that may be licensed from third parties.

If you would like to use or distribute our Springer Nature journal content to a wider audience or on a regular basis or in any other manner not expressly permitted by these Terms, please contact Springer Nature at

onlineservice@springernature.com